

Efficient calculation of three-dimensional tensor networks

Li-Ping Yang,¹ Y. F. Fu,² Z. Y. Xie,^{2,*} and T. Xiang^{3,4,5,†}

¹*Department of Physics, Chongqing University, Chongqing 401331, China*

²*Department of Physics, Renmin University of China, Beijing 100872, China*

³*Institute of Physics, Chinese Academy of Sciences, Beijing, 100190, China*

⁴*Beijing Academy of Quantum Information Sciences, Beijing 100193, China*

⁵*University of Chinese Academy of Sciences, Department of Physics, Beijing 100190, China*

We have proposed an efficient algorithm to calculate physical quantities in the translational invariant three-dimensional tensor networks, which is particularly relevant to the study of the three-dimensional classical statistical models and the (2+1)-dimensional quantum lattice models. In the context of a classical model, we determine the partition function by solving the dominant eigenvalue problem of the transfer matrix, whose left and right dominant eigenvectors are represented by two projected entangled simplex states. These two projected entangled simplex states are not hermitian conjugate to each other but are appropriately arranged so that their inner product can be computed much more efficiently than in the usual prescription. For the three-dimensional Ising model, the calculated internal energy and spontaneous magnetization agree with the published results in the literature. The possible improvement and extension to other models are also discussed.

I. INTRODUCTION

The many-body problem is one of the central problems in physics, and developing accurate and efficient numerical methods that can effectively handle the exponential growth of the corresponding Hilbert space has always been a great challenge, especially for quantum systems. Based on the idea of renormalization group as well as the tensor-network representation of partition functions and wave functions, tensor-network methods have evolved progressively to be an important member of many-body computational methods in recent years [1–3]. In fact, due to the absence of sign problem and the ability to deal with two-dimensional systems, tensor networks are drawing increasing attention, and have been applied successfully to strongly-correlated electron systems [4, 5], frustrated spin systems [6–9], statistical models [10–12], topological order [13–16], quantum field theory [17–19], machine learning [20, 21], and even quantum circuit simulation [22], etc. Among the various tensor-network methods, imaginary time evolution is a highly efficient method to determine the ground state of low-dimensional quantum systems [3, 23, 24].

A central task in the application of tensor network states to 2+1 dimensional quantum lattice models, is to contract a two-dimensional tensor network, which has double-layer structure and bond dimension D^2 , with D the maximal virtual bond dimension of the tensor network representation of a quantum state [3]. This is extremely costly, and thus though D is expected to be larger in order to give more accurate result, it is limited to about 13 in practical calculations [9, 16, 25]. There are some efforts in recent years to solve this problem, such as employing symmetries [26, 27], combining Monte Carlo

sampling [28], and the nested tensor network method [29]. However, apparently the problem is not completely solved, and developing efficient algorithms to resolve this issue is still an important topic for tensor-network communities.

At the meanwhile, it is known that, in the formalism of path integral, the equilibrium quantum many-body problem in d dimensions is similar to the classical many-body problem in $d+1$ dimensions. Thus inspired by the success in one- and two-dimensional quantum systems, there are also some efforts of applying tensor-network methods to three-dimensional (3D) classical models. Actually, both the coarse-graining tensor renormalization group algorithms [10, 30–32] and the transfer-matrix-based tensor-network state methods [33–39] have been applied to these models or related previously. Though the transfer-matrix-based methods can work excellently in two-dimensional networks, it seems that they are not so efficient in three dimensions. For example, the variational optimization procedure seems indispensable, and bond dimension of the involved tensor-network states and thus the accuracy are limited. Especially, as far as we know, whether a simple algorithm analogous to imaginary time evolution in two-dimensional quantum lattice models can be developed for 3D classical models is unclear up to now.

In this work, we are trying to address the issues. To be specific, following the usual prescription of the transfer-matrix-based methods, we firstly express the partition function of a 3D classical model in terms of some special two-dimensional transfer matrices, and reduce the problem to the dominant eigenvalue problem of the matrices. Then we solve the dominant eigenvalue problem by representing the dominant eigenvector as a special tensor-network state, namely the projected entangled simplex state (PESS) [25], which is efficiently determined through a power iteration procedure analogous to imaginary time evolution, as done for two-dimensional classical models similarly [40]. In particular, a simple nesting technique

* qingtaoxie@ruc.edu.cn

† txiang@iphy.ac.cn

is proposed in which the PESS representations of the left and right dominant eigenvectors are designed appropriately so that their inner-product can be expressed as a tensor network with bond dimension D instead of D^2 , and thus the contraction can be carried out much more efficiently. Combining this nesting technique with the corner transfer matrix renormalization group (CTMRG) algorithm [4, 41, 42], we are able to push the bond dimension D to 20 in this work. For the 3D Ising model, it shows that even if the tensor network state is renormalized by the so-called simple update technique [24, 25, 43] after each evolution step, the obtained local quantities, such as energy density and spontaneous magnetization, are in good consistent with the previous studies, and the estimated critical temperature T_c is about 4.5100(5) which has only a relative deviation of about 10^{-4} from the best Monte Carlo estimations.

The rest of the paper is organized as follows. In Sec. II, we introduce some details of the algorithm employed in this work, especially the nesting technique. The numerical results for statistical averages, such as energy density E and spontaneous magnetization M , as well as the convergence analysis, are presented in Sec. III. In Sec. IV, we summarize our work, and discuss the possible improvement and promising extensions briefly.

II. METHOD

A. Tensor-network representation of the partition function

For concreteness, hereinafter we will focus on the 3D Ising model. The partition function can be written as

$$Z = \sum_{\{s\}} \prod_{\langle ij \rangle} e^{\beta s_i s_j}, \quad (1)$$

where $s_i = \pm 1$ is the spin variable located on the i -th lattice site, β is the inversed temperature, $\langle ij \rangle$ means the product is performed over all the nearest neighboring bonds, and the summation is over all the spin configurations.

For later use, we regroup the product in Eq. (1) in unit of cube that is the building block of a cubic lattice, i.e.,

$$Z = \sum_{\{s\}} \prod_{\alpha} T^{(\alpha)}, \quad (2)$$

where $T^{(\alpha)}$ is a rank-8 tensor defined at the α -th cube. E.g., as shown in right panel of Fig. 1, for a cube where the spin variables residing on the eight vertices are denoted by s_1 - s_8 , the local tensor T can be expressed as the following product of twelve Boltzmann weights corresponding to each edge of the cube, respectively,

$$\begin{aligned} T_{s_1 s_2 s_3 s_4 s_5 s_6 s_7 s_8} &= \exp [\beta (s_1 s_2 + s_2 s_3 + s_3 s_4 + s_4 s_1 + s_5 s_6 + s_6 s_7 + \\ & s_7 s_8 + s_8 s_5 + s_1 s_5 + s_2 s_6 + s_3 s_7 + s_4 s_8)]. \end{aligned} \quad (3)$$

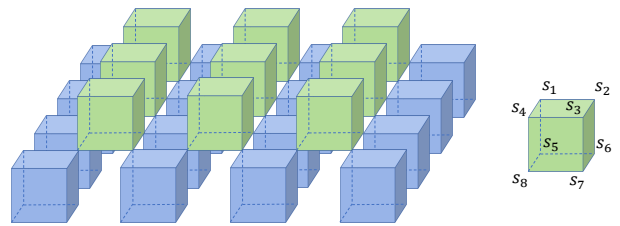


FIG. 1. Special transfer matrices in the expression of partition function of 3D Ising model. (left) The green and blue cubes constitute transfer matrices T_2 and T_1 , as expressed in Eq. (4) and (5). (right) The definition of local tensor T located in each colored cube, as expressed in Eq. (3). As mentioned in the main text, the vertical direction is referred to as z -direction for convenience.

Manifestly, to make Eq. (2) and (3) consistent, T should be defined only in two kinds of inequivalent cubes, as denoted as green and blue, respectively, in the left panel of Fig. 1. Thus the two kinds of cubes form an alternative or staggered structure in vertical direction. This is very similar to the case of the imaginary time evolution in quantum lattice models, where the trotter-suzuki decomposition of the evolution operator $e^{-\tau H}$ always leads to an alternative structure in imaginary time τ -direction. In the following, we will use this special structure extensively. For convenience, the vertical direction will be referred to as z -direction hereinafter.

B. Determination of the tensor-network representation of the dominant eigenvector

Following the prescription of the transfer-matrix-based method, one need to express the partition function in terms of some transfer matrices. To this end, we firstly introduce two tensor-network operators

$$T_1 = \bigotimes_{\alpha \in b} T^{(\alpha)}, \quad T_2 = \bigotimes_{\alpha \in g} T^{(\alpha)}, \quad (4)$$

where the direct products are performed over T s defined at *blue* cubes and *green* cubes, respectively, as illustrated in Fig. 1. And then we can identify the following equality

$$Z = \text{Tr} (T_2 T_1)^{2n}, \quad (5)$$

where the length in the z -direction is denoted as $2n$ for convenience. It is worth noting that T_1 and T_2 should be understood as matrices by grouping indices properly in Eq. (4) and (5), in order to make the operations for matrices therein meaningful.

Once Eq. (5) is established, the calculation of partition function is immediately reduced to the dominant eigenvalue problem of the transfer matrix $T_2 T_1$, which can be solved by power iteration method and is very similar

to the imaginary time evolution. In this work, we represent the corresponding dominant eigenvector $|\Psi\rangle$ as a projected entangled simplex state [25, 44], which can be written as

$$|\Psi\rangle = \sum_{\{s\}} \text{Tr}(\dots A_{a_\alpha b_\alpha c_\alpha d_\alpha}^{(\alpha)} B_{a_\beta b_\beta c_\beta d_\beta}^{(\beta)} P_{a_i b_i}^{(i)} [s_i] \dots) |\dots s_i \dots\rangle, \quad (6)$$

as illustrated in Fig. 2. Here α and β denotes the coordinates of two inequivalent squares, at the center of which a rank-4 simplex tensor A or B is introduced to characterize the four-spin entanglement in that square. i denotes the coordinates of lattice sites, where a rank-3 projection tensor P is defined with two virtual indices labeled as a, b, c, \dots and a single physical index labeled as s . Every two virtual indices associated with the same bond take the same values. Tr is over all the repeated virtual indices and \sum is over all the spin configurations $\{s\}$.

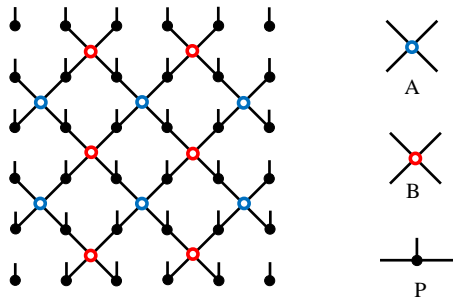


FIG. 2. Tensor network representation of the dominant eigenvector of the transfer matrix T_2T_1 appeared in Eq. (5), as formulated in Eq. (6). The black vertical lines denote the physical configurations $\{s\}$ appeared in Eq. (6).

Due to the similar alternative structure to the time-evolution operators in quantum lattice models, we can take the same strategy to determine the variational parameters A , B , and P in $|\Psi\rangle$. To be specific, starting from a random state $|\Psi_0\rangle$ which has the same structure as $|\Psi\rangle$, we apply T_1 and T_2 alternatively to $|\Psi_0\rangle$ and update the parameters accordingly by local decompositions of the related clusters after each projection. This procedure is applied repeatedly until the convergence is reached, and the obtained tensor network state provides an approximate representation of $|\Psi\rangle$. In essence, the method described here is equivalent to the simple update method [24, 25, 43] developed in quantum systems, and has been applied to two-dimensional classical models under the help of canonical form of matrix product state [40]. Fig. 3 illustrates how a single projection step is performed. For more details, we suggest referring to Ref. [25].

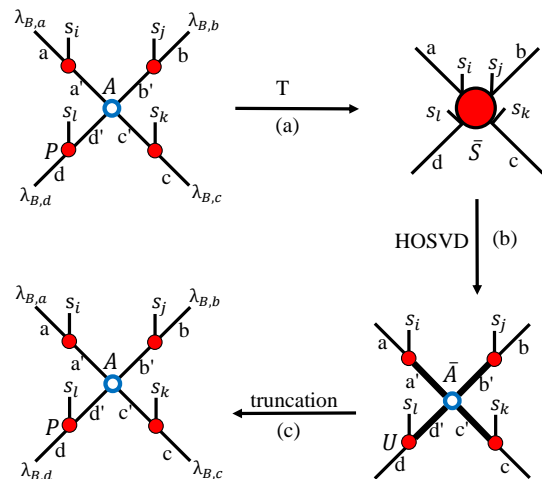


FIG. 3. A single projection step of T on the PESS ansatz, as described in the main text. The positive definite vector λ_B is obtained from the higher-order singular value decomposition of the B tensor. For more details, one can refer to the elaboration in Ref. [25].

C. Nesting structure of inner product between the left and right dominant eigenvectors

To describe the nesting technique developed in this work, firstly we briefly describe how the statistical averages are obtained in the traditional reduced tensor network method [3, 29]. As long as the dominant eigenvector $|\Psi\rangle$ is obtained, we can use the fundamental formula to calculate the statistical averages of local physical quantities. E.g., the average magnetization located at i -th site can be determined by

$$M_i = \frac{\sum_{\{s\}} s_i \prod_{\alpha} T^{(\alpha)}}{\sum_{\{s\}} \prod_{\alpha} T^{(\alpha)}} = \frac{\text{Tr}(T_2T_1)^n s_i (T_2T_1)^n}{\text{Tr}(T_2T_1)^n (T_2T_1)^n}, \quad (7)$$

where we have used the transfer-matrix expression of Z and assumed that s_i sits in the middle of z -direction. In the thermodynamic limit, $n \rightarrow \infty$, and we reach

$$M_i = \frac{\langle \Psi' | s_i | \Psi \rangle}{\langle \Psi' | \Psi \rangle}, \quad M = \frac{\sum_{i \in \alpha} M_i}{8}, \quad (8)$$

where $\langle \Psi' |$ is the left dominant eigenvector of T_2T_1 and can be derived easily due to the symmetry between T_1 and T_2 . The spontaneous magnetization M is obtained eventually as above by averaging over the eight spins in the same cube due to the translational invariance of the tensor networks. Internal energy E of the bonds lying in xy -planes can be obtained similarly, while for bonds in z -direction, we can follow the widely-used impurity method as discussed in Refs. [26, 43, 45].

As indicated explicitly in Eq. (8), the statistical average of a local physical quantity needs to contract a two-dimensional tensor network, which is identical to the expectation value calculation for quantum lattice models

in essence. If $|\Psi\rangle$ has bond dimension D , then the generated two-dimensional tensor network has dimension D^2 , as shown in Fig. 4, and can be contracted by the CTMRG algorithm [4, 41, 42] effectively, when D is small.

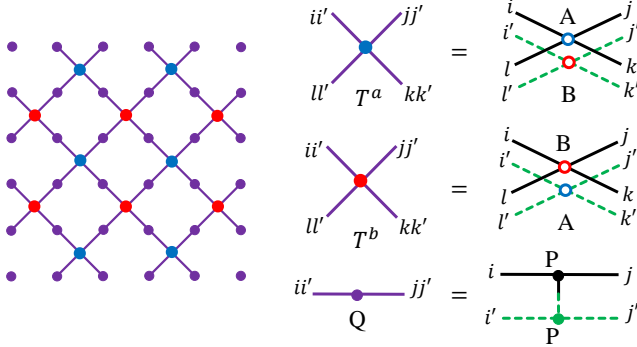


FIG. 4. Sketch of $\langle\Psi'|\Psi\rangle$ appeared in Eq. (8). Here $\langle\Psi'$ is the left dominant eigenvector of T_2T_1 . The relevance to $|\Psi\rangle$ and thus the structure of the local tensors T^a and T^b , come from the symmetry between T_1 and T_2 .

However, contracting a two-dimensional tensor network with bond dimension D^2 is extremely costly when D is large, and thus one can use the nested tensor network technique [29] to improve the efficiency of conventional contraction methods. Nevertheless, in this work, we did not take this strategy, instead, we proposed a much simpler nesting technique by taking advantage of the special cubic lattice structure. This nesting technique can reduce the computational cost similarly as achieved by the nested tensor network method, keeps the symmetry of the ground state properly, and is especially suitable for cubic systems.

To see how it works, we firstly divide the cubic lattice into three parts, namely two bulks whose contribution to the full partition function can be expressed in terms of transfer matrices, and the surface part which connects the two bulks and combines as the whole cubic lattice. This means we have rewritten the partition function in another manner, as illustrated in Fig. 5(a),

$$Z = \text{Tr}(T_4T_3)^n XVY(T_2T_1)^n, \quad (9)$$

where T_1 and T_2 are the transfer matrices corresponding to the lower bulk, T_3 and T_4 correspond to the upper bulk similarly, and X , Y , V are auxiliary matrices to describe the surface part. Here we intentionally decompose the lower and upper part in different manners, and their relative locations projected in xy -plane are shown in Fig. 5(b). Mathematically,

$$X = \prod_{\langle ij \rangle_t \notin g} e^{\beta s_i s_j}, \quad Y = \prod_{\langle ij \rangle_b \notin o} e^{\beta s_i s_j}, \quad V = \prod_{\langle ij \rangle_{bt}} e^{\beta s_i s_j}, \quad (10)$$

which are explicitly shown in Fig. 5(a). Here X and Y can be understood as onsite diagonal matrices, $\langle ij \rangle_t \notin g$

means the product is over the nearest spin pairs between green cubes on the top surface of lower bulk, and $\langle ij \rangle_b \notin o$ means the product is over the nearest spin pairs between orange cubes at the bottom surface of upper bulk. $\langle ij \rangle_{bt}$ means V is the product of Boltzmann weights corresponding to all the bonds connecting the two bulks in z -direction. In Fig. 5(a), the dashed bonds corresponding to X , Y , and V , are denoted as black, blue, and red, respectively. Note in Eq. (9), the size in z -direction is assumed as $2n+1$ for convenience.

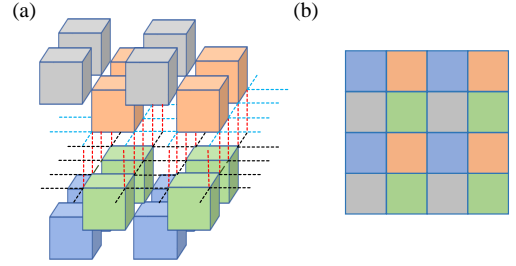


FIG. 5. Decomposition of the cubic lattice into three parts, as described in the nesting technique in Sec. II. (a) The cubes with color blue, green, orange and grey, constitute the transfer matrices T_1 , T_2 , T_3 , and T_4 , respectively. The dashed lines with color black, blue, and red, constitute the transfer matrices X , Y , and V , respectively. The full partition function can be represented in terms of these transfer matrices, as expressed in Eq. (9). (b) The spatial distribution of the cubes in xy -plane, for the sixteen cubes shown in (a).

In the thermodynamic limit, the evaluation of Eq. (9) is again reduced to the dominant eigenvalue problem as before, and the statistical averages can be determined similarly. For example, the bond energy in z -direction can be obtained by

$$E_p = \frac{\langle\Phi|XV'Y|\Psi\rangle}{\langle\Phi|XVY|\Psi\rangle}, \quad V' = (-s_a s_b e^{\beta s_a s_b}) \prod_{\langle ij \rangle_{bt} \neq p} e^{\beta s_i s_j}, \quad (11)$$

where $\langle\Phi|$ is the left dominant eigenvector of T_4T_3 , and V' differs from V by only a single vertical bond denoted as p with s_a and s_b located at its ends. Finally we have

$$E_p = \frac{\langle\tilde{\Phi}|V'|\tilde{\Psi}\rangle}{\langle\tilde{\Phi}|V|\tilde{\Psi}\rangle}, \quad \langle\tilde{\Phi}| \equiv \langle\Phi|X, \quad |\tilde{\Psi}\rangle \equiv Y|\Psi\rangle, \quad (12)$$

The key observation is that $\langle\tilde{\Phi}|$ and $|\tilde{\Psi}\rangle$ have similar structure but the parameters are distributed separately in space, which can be seen from Fig. 5(b) straightforwardly. And this leads to a great advantage, i.e., if the wavefunctions $\langle\tilde{\Phi}|$ and $|\tilde{\Psi}\rangle$ are approximated by PESS with bond dimension D , then the generated two-dimensional tensor network has also bond dimension D , instead of D^2 . E.g., as to the denominator, exploring the symmetry between $\langle\tilde{\Phi}|$ and $|\tilde{\Psi}\rangle$, the resulting tensor network are composed of three parameters, i.e., the original parameters A , B in $|\Psi\rangle$ and $|\Phi\rangle$, and a new local

tensor T^p derived from P therein, i.e.,

$$T_{ijkl}^p = \sum_{s_a s_b} P_{lj}[s_a] P_{ki}[s_b] e^{\beta s_a s_b}, \quad (13)$$

as illustrated in Fig. 6. Therefore, compared with the reduced method which generates a tensor network with squared bond dimension, this nesting technique can greatly reduce the cost and leads to much more efficient contraction, as achieved in Ref. [29] similarly. In this work, we push D to 20 with the help of this technique.

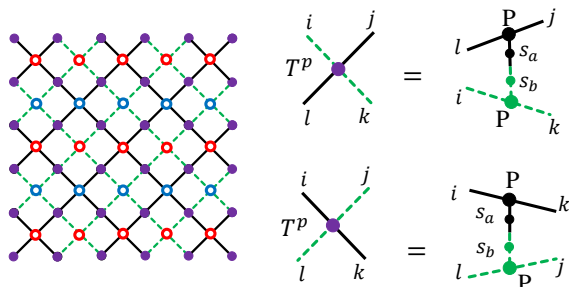


FIG. 6. Sketch of $\langle \tilde{\Phi} | V | \tilde{\Psi} \rangle$ appeared in Eq. (12). The virtual bonds in $\langle \tilde{\Phi} |$ and $| \tilde{\Psi} \rangle$ are indicated as solid black and dashed green lines, respectively. Here we have used the symmetry between the two wavefunctions, and both the two definitions of T^p hold, as expressed in Eq. (13), though it is unnecessary. The tensors A , B and P are the parameters in $| \tilde{\Psi} \rangle$ in this context. Clearly the bond dimension of the resulting tensor network is not squared which is different from the case in Fig. 4.

III. RESULTS

In this work, we focus on the 3D Ising model, which is of long-standing interest in statistical physics and condensed matter physics. Though there is no analytical solution as in two-dimensional case, the higher-order tensor renormalization group (HOTRG) [10, 46] and Monte Carlo methods [47–50] have provided very accurate numerical data which confirms a second-order finite temperature phase transition. Therefore, this model provides a suitable touchstone to test new numerical algorithms in higher dimensions.

In this work, as described in Sec. II, we use the developed evolution method combined with the simple update technique to determine the tensor-network representation of the dominant eigenvectors of the transfer matrices. For $D > 10$, we employ the nesting technique described in Sec. II C to improve the efficiency of CTMRG algorithm.

The result of internal energy E is shown in Fig. 7. The reference curve denotes the data from HOTRG calculation with $D = 14$, which gives very consistent specific heat with the well-accepted Monte Carlo data in the literature, as shown in Ref. [10]. It seems that the proposed method can give consistent result off the critical region,

while near the critical point, enlarging the bond dimension D can produce more accurate result as expected. The spontaneous magnetization M shows similar behavior, as shown in Fig. 8, where the reference curve is obtained from Monte Carlo [47]. For both the two quantities, our result coincides well with previous studies, and the singular behavior can be seen clearly.

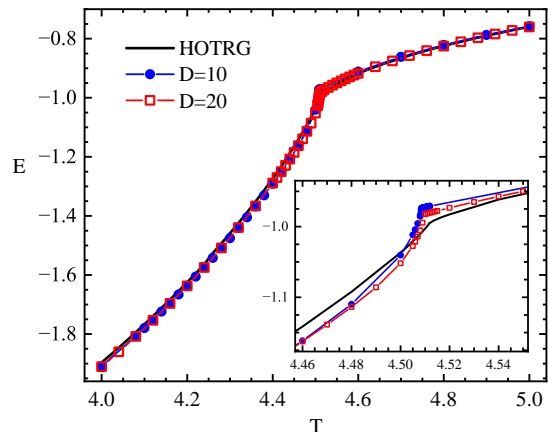


FIG. 7. Energy estimation obtained from $D = 20$ and $\chi = 120$. The HOTRG data from Ref. [10] with $D = 14$ are plotted as a reference.

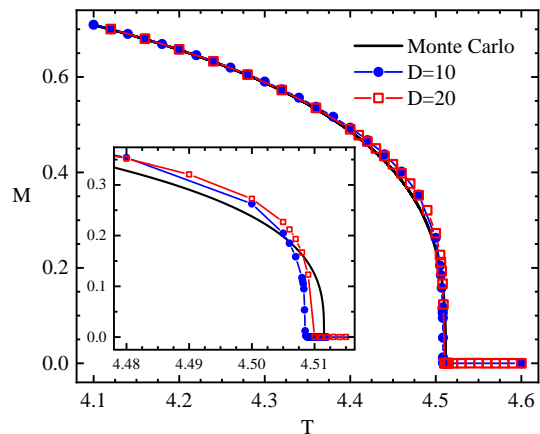


FIG. 8. Magnetization estimation obtained from $D = 20$ and $\chi = 120$. The Monte Carlo data from Ref. [47] are plotted as a reference.

From E and M , and the critical temperatures derived as shown in Fig. 9, it seems that the proposed method tends to underestimate the critical temperature a little bit, which is different from the coarse-graining tensor renormalization group methods as shown, e.g., in Refs. [10, 51]. This is probably related to the simple

update technique used in the evolution process, since it essentially provides a Bethe lattice approximation of the dominant eigenvector [52, 53] and thus tends to be disordered at finite temperature, especially at temperature close to but lower than critical point where the approximation cannot give a good estimate of the correlation length. When $D = 20$, the estimated critical temperature T_c is about 4.5100(5), which has only about 10^{-4} relative deviation from the best estimation $T_c \sim 4.51152$ [10, 46, 50].

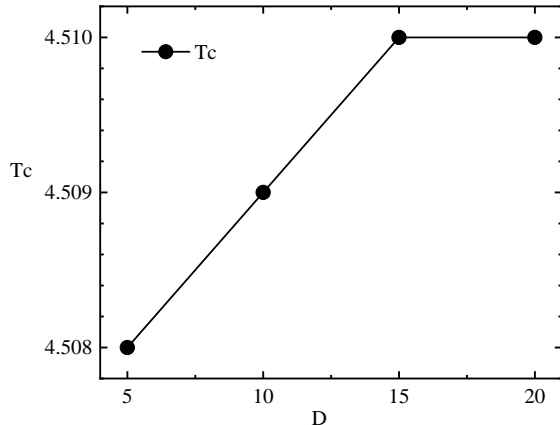


FIG. 9. Critical temperature obtained from the magnetization M , with respect to the bond dimension D of the tensor network state representation of the transfer matrices' dominant eigenvectors.

As to the new nesting technique proposed in this work, its convergence with respect to the bond dimension χ of the environment tensors used in CTMRG is shown in Fig. 10, for $D = 20$. It shows that for all the three typical temperatures ranging from symmetry-breaking phase to paramagnetic phase, the convergence is at least equally satisfying, compared with the nested tensor network method proposed in Ref. [29]. Particularly, even at temperature that is very close to the critical value, the convergence is already very acceptable when $\chi = 180$ for $D = 20$, with an error about 10^{-6} for E and 10^{-4} for M . This is a very nice feature for tensor-network methods, especially for large D , as discussed in Ref. [29] in detail.

IV. SUMMARY

In this paper, we propose an efficient numerical method to contract the 3D tensor networks with translational invariance. The result of the contraction is expressed in terms of some transfer matrices, whose dominant eigenvectors are represented as the PESS form and determined by power iterations analogous to the imaginary time evolution algorithm [23, 40]. Especially, the PESS represen-

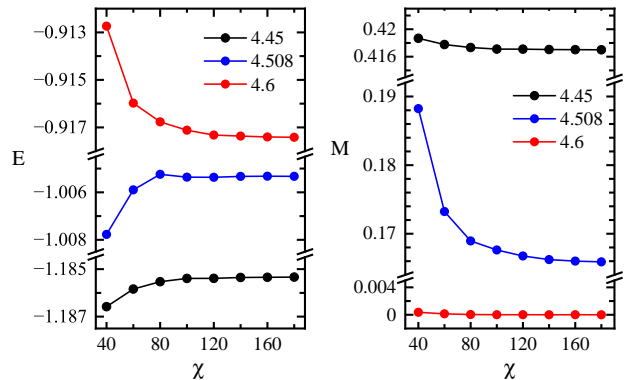


FIG. 10. Convergence analysis about energy and magnetization for $D = 20$. Three typical temperatures are chosen, i.e., temperature in symmetry-breaking phase (4.45), close to critical point (4.508), and in disordered phase (4.6).

tations of the left and right dominant eigenvectors are designed appropriately so that their inner-product has a nesting structure and can be expressed as a tensor network with bond dimension D instead of D^2 , and thus the contraction can be carried out much more efficiently. As to the 3D Ising model, it can give very consistent result for both energy and magnetization with previous studies, even the simple update strategy is employed to update the tensor network states. The convergency of the nesting technique is shown to be at least equally good to that of the nested tensor network method [29]. When $D = 20$, we obtain a critical temperature about 4.5100(5) which is very close to the best known estimation. As far as we know, this is probably the first successful trial of applying the imaginary-time-evolution-like method to 3D classical models without variational update procedure, and thus extend the application scope of tensor network states. The applications to other interesting but unsolvable classical models in three dimensions, such as Potts model [46], clock model [54], dimer model [38], and lattice gauge models [55], are straightforward.

As mentioned in Sec. III, the simple update strategy employed in this work is probably a reason why the obtained T_c tends to be underestimated. Besides the scaling hypothesis and data collapse technique [39], this tendency could be eased in two different manners. One is to resort to the more involved but more accurate update methods, such as the cluster update [56] and the full update strategies [57, 58], which consider renormalization effect of the environment better. The other possible way is to utilize more sophisticated ansatz and evolution techniques, such as PESS ansatz with stronger simplex entanglement [25], the recently proposed regularized scheme of time evolution [59], and the so-called minimal canonical form of tensor network states [60], all of which are also expected to produce more accurate representation of the dominant eigenvectors. In both cases, the nesting technique proposed in this work can still be applied without

change, and the improvement of performance can be expected arguably.

At last, it is worth mentioning that the proposed nesting technique in this work can be also extended to the two-dimensional quantum lattice models. In order to achieve this, one need to represent the partition function in a different manner, e.g., similarly as we have done in Eq. (9), so that two representations of the ground state with separated distributions in space can be used simultaneously, e.g., as illustrated in Fig. 5(b) and expressed in Eq. (12). This can be advantageous in the study of models which have square structure and separatable block interactions, such as Shastry-Sutherland model [6, 61], checkboard system [62], and so on. Exploring its potential and limit is an interesting and promising topic, and

we would like to leave it as a future pursuit.

ACKNOWLEDGEMENT

We thank Zhong-Cao Wei and Zhi-Yuan Liu for their contribution in the early stage of this work. We are supported by the National R&D Program of China (Grants No. 2017YFA0302900 and No. 2016YFA0300503), the National Natural Science Foundation of China (Grants Nos. 12274458, 11888101, 11874095, and 11774420), and by the Research Funds of Renmin University of China (Grants No. 20XNLG19). Li-Ping Yang and Y. F. Fu contribute equally to this work.

-
- [1] F. Verstraete and J. I. Cirac, arXiv:0407066 (2004); J. I. Cirac, D. P. Garcia, N. Schuch, and F. Verstraete, *Rev. Mod. Phys.* **93**, 045003 (2021).
 - [2] S. Montangero, *Introduction to Tensor Network Methods*, Springer (2018).
 - [3] R. Orus, *Ann. Phys.* **349**, 117 (2014); R. Orus, *Eur. Phys. J. B* **87**, 280 (2014); R. Orus, *Nat. Rev. Phys.* **1**, 538 (2019).
 - [4] P. Corboz, T. M. Rice, and M. Troyer, *Phys. Rev. Lett.* **113**, 046402 (2014).
 - [5] Simons Collaboration on the Many-Electron Problem, *Phys. Rev. X* **5**, 041041 (2015), and *Phys. Rev. X* **10**, 031016 (2020); B. X. Zheng, et al., *Science* **358**, 1155 (2017).
 - [6] P. Corboz and F. Mila, *Phys. Rev. Lett.* **112**, 147203 (2014); P. Corboz and F. Mila, *Phys. Rev. B* **87**, 115144 (2013).
 - [7] L. Wang, Z. C. Gu, F. Verstraete, and X. G. Wen, *Phys. Rev. B* **94**, 075143 (2016).
 - [8] H. J. Liao, Z. Y. Xie, J. Chen, Z. Y. Liu, H. D. Xie, R. Z. Huang, B. Normand, and T. Xiang, *Phys. Rev. Lett.* **118**, 137202 (2017).
 - [9] Q. Li, H. Li, J. Z. Zhao, H. G. Luo, and Z. Y. Xie, *Phys. Rev. B* **105**, 184418 (2022).
 - [10] Z. Y. Xie, J. Chen, M. P. Qin, J. W. Zhu, L. P. Yang, and T. Xiang, *Phys. Rev. B* **86**, 045139 (2012).
 - [11] C. Wang, S. M. Qin, and H. J. Zhou, *Phys. Rev. B* **90**, 174201 (2014).
 - [12] J. G. Liu, L. Wang, and P. Zhang, *Phys. Rev. Lett.* **126**, 090506 (2021).
 - [13] C. Wille, O. Buerschaper, and J. Eisert, *Phys. Rev. B* **95**, 245127 (2017).
 - [14] W. T. Xu, Q. Zhang, and G. M. Zhang, *Phys. Rev. Lett.* **124**, 130603 (2020).
 - [15] D. J. Williamson, N. Bultinck, and F. Verstraete, arXiv:1711.07982.
 - [16] R. Wang, Z. Y. Xie, B. G. Wang, and T. Sedrakyan, *Phys. Rev. B* **106**, L121117 (2022).
 - [17] F. Verstraete and J. I. Cirac, *Phys. Rev. Lett.* **104**, 190405 (2010).
 - [18] Y. Z. Liu, Y. Meurice, M. P. Qin, J. Unmuth-Yockey, T. Xiang, Z. Y. Xie, J. F. Yu, and H. Y. Zou, *Phys. Rev. D* **88**, 056005 (2013).
 - [19] A. Tilloy and J. I. Cirac, *Phys. Rev. X* **9**, 021040 (2019).
 - [20] Z. Y. Han, J. Wang, H. Fan, L. Wang, and P. Zhang, *Phys. Rev. X* **8**, 031012 (2018).
 - [21] Z. F. Gao, S. Cheng, R. Q. He, Z. Y. Xie, H. H. Zhao, Z. Y. Lu, and T. Xiang, *Phys. Rev. Research* **2**, 023300 (2020).
 - [22] Y. Meurice, R. Sakai, and J. Unmuth-Yockey, *Rev. Mod. Phys.* **94**, 025005 (2022).
 - [23] G. Vidal, *Phys. Rev. Lett.* **91**, 147902 (2003); *Phys. Rev. Lett.* **93**, 040502 (2004).
 - [24] G. Vidal, *Phys. Rev. Lett.* **98**, 070201 (2007).
 - [25] Z. Y. Xie, J. Chen, J. F. Yu, X. Kong, B. Normand, and T. Xiang, *Phys. Rev. X* **4**, 011025 (2014).
 - [26] H. H. Zhao, Z. Y. Xie, Q. N. Chen, Z. C. Wei, J. W. Cai, and T. Xiang, *Phys. Rev. B* **81**, 174411 (2010).
 - [27] P. Schmoll, S. Singh, M. Rizzi, and R. Orus, *Ann. Phys.* **419**, 168232 (2020); M. Mambrini, R. Orus, and D. Poilblanc, *Phys. Rev. B* **94**, 205124 (2016).
 - [28] L. Wang, I. Pizorn, and F. Verstraete, *Phys. Rev. B* **83**, 134421 (2011); W.-Y. Liu, S.-J. Dong, Y.-J. Han, G.-C. Guo, and L. X. He, *Phys. Rev. B* **95**, 195154 (2017); H.-H. Zhao, K. Ido, S. Morita, and M. Imada, *Phys. Rev. B* **96**, 085103 (2017).
 - [29] Z. Y. Xie, H. J. Liao, R. Z. Huang, H. D. Xie, J. Chen, Z. Y. Liu, and T. Xiang, *Phys. Rev. B* **96**, 045128 (2017).
 - [30] P. Y. Teng, *Physica A* **472**, 117 (2017).
 - [31] D. Kadoh, and K. Nakayama, arXiv:1912.02414.
 - [32] D. Adachi, T. Okubo, and S. Todo, *Phys. Rev. B* **102**, 054432 (2020).
 - [33] T. Nishino and K. Okunishi, *J. Phys. Soc. Jpn.* **67**, 3066 (1998).
 - [34] K. Okunishi and T. Nishino, *Prog. Theor. Phys.* **103**, 541 (2000); T. Nishino, K. Okunishi, Y. Hieida, N. Maeshima, and Y. Akutsu, *Nucl. Phys. B* **575**, 504 (2000); A. Gendiar and T. Nishino, *Phys. Rev. E* **65**, 046702 (2002).
 - [35] T. Nishino, Y. Hieida, K. Okunishi, N. Maeshima, Y. Akutsu, and A. Gendiar, *Prog. Theor. Phys.* **105**, 409 (2001); A. Gendiar, N. Maeshima, and T. Nishino, *Prog. Theor. Phys.* **110**, 691 (2003).
 - [36] S. G. Chung, *Phys. Lett. A* **359**, 707 (2006).
 - [37] R. Orus, *Phys. Rev. B* **85**, 205117 (2012).

- [38] L. Vanderstraeten, B. Vanhecke, and F. Verstraete, *Phys. Rev. E* **98**, 042145 (2018).
- [39] B. Vanhecke, J. Hasik, F. Verstraete, and L. Vanderstraeten, arXiv:2102.03143.
- [40] R. Orus, and G. Vidal, *Phys. Rev. B* **78**, 155117 (2008).
- [41] T. Nishino and K. Okunishi, *J. Phys. Soc. Jpn.* **65**, 891 (1996).
- [42] R. Orús and G. Vidal, *Phys. Rev. B* **80**, 094403 (2009).
- [43] H. C. Jiang, Z. Y. Weng, and T. Xiang, *Phys. Rev. Lett.* **101**, 090603 (2008).
- [44] N. Schuch, D. Poilblanc, J. I. Cirac, and D. P. Garcia, *Phys. Rev. B* **86**, 115108 (2012).
- [45] H. H. Zhao, Z. Y. Xie, T. Xiang, and M. Imada, *Phys. Rev. B* **93**, 125115 (2016).
- [46] S. Wang, Z. Y. Xie, J. Chen, B. Normand, and T. Xiang, *Chin. Phys. Lett.* **31**, 070503 (2014).
- [47] A. L. Talapov and H. W. J. Blote, *J. Phys. A: Math. Gen.* **29**, 5727 (1996).
- [48] Y. J. Deng and H. W. J. Blote, *Phys. Rev. E* **68**, 036125 (2003); X. M. Feng and H. W. J. Blote, *Phys. Rev. E* **81**, 031103 (2010).
- [49] M. Hasenbusch, *Phys. Rev. B* **82**, 174433 (2010).
- [50] A. M. Ferrenberg, J. Xu, and D. P. Landau, *Phys. Rev. E* **97**, 043301 (2018).
- [51] Z. Y. Xie, H. C. Jiang, Q. N. Chen, Z. Y. Weng, and T. Xiang, *Phys. Rev. Lett.* **103**, 160601 (2009).
- [52] W. Li, J. von Delft, and T. Xiang, *Phys. Rev. B*, **86**, 195137 (2012).
- [53] H. J. Liao, Z. Y. Xie, J. Chen, X. J. Han, H. D. Xie, B. Normand, and T. Xiang, *Phys. Rev. B*, **93**, 075154 (2016).
- [54] H. Shao, W. Guo, and A. W. Sandvik, *Phys. Rev. Lett.* **124**, 080602 (2020).
- [55] Y. Z. Liu, Y. Meurice, M. P. Qin, J. U. Yockey, T. Xiang, Z. Y. Xie, J. F. Yu, and H. Zou, *Phys. Rev. D* **88**, 056005 (2013).
- [56] L. Wang, and F. Verstraete, arXiv:1110.4362; L. Wang, Z. C. Gu, F. Verstraete, and X. G. Wen, *Phys. Rev. B* **94**, 075143 (2016).
- [57] J. Jordan, R. Orus, G. Vidal, F. Verstraete, and J. I. Cirac, *Phys. Rev. Lett.* **101**, 250602 (2008); R. Orus and G. Vidal, *Phys. Rev. B* **80**, 094403 (2009).
- [58] M. Lubasch, J. I. Cirac, and M. C. Banuls, *Phys. Rev. B* **90**, 064425 (2014); H. N. Phien, J. A. Benghua, H. D. Tuan, P. Corboz, and R. Orus, *Phys. Rev. B* **92**, 035142 (2015).
- [59] L. X. Cen, arXiv:2208.03436.
- [60] A. Acuaviva, V. Makam, H. Nieuwboer, D. P. Garcia, F. Sittner, M. Walter, and F. Witteveen, arXiv:2209.14358.
- [61] B. S. Shastry and B. Sutherland, *Physica* **108B**, 1069 (1981); J. Yang, A. W. Sandvik, and L. Wang, *Phys. Rev. B* **105**, L060409 (2022).
- [62] H. Y. Zou, F. Yang, and W. Ku, arXiv:2011.06520.